AAPS PharmSciTech (2024) 25:148
https://doi.org/10.1208/s12249-024-02852-4

RESEARCH ARTICLE

Mucoadhesive Chitosan Composite Sponge as a Carrier for β-Sitosterol Cubosomes for Thermal Burn Treatment

Abeer Khattab[1] · **Soha Ismail**[1] · **Areeg M. Abd-Elrazek**[2]

Received: 21 February 2024 / Accepted: 23 May 2024 / Published online: 27 June 2024

Abstract

Our study aimed to explore the potential of using nanostructured lipid carriers (NLCs) to enhance the topical administration of β-sitosterol, a bioactive that is poorly soluble in water. Here, we have taken advantage of the unique characteristics that cubosomes have to provide as a drug delivery system. These characteristics include a large surface area, thermal stability, and the capacity to encapsulate molecules that are hydrophobic, amphiphilic, and hydrophilic. The cubosomal formulation was optimized by building a central composite design. The optimum dispersion exhibited a particle size of 88.3 nm, a zeta potential of -43, a polydispersity index of 0.358, and drug entrapment of 95.6%. It was composed of 15% w/w oleic acid and 5% w/w pluronic F127. The optimized cubosome dispersion was incorporated into a sponge formulation. The optimized cubosome sponge achieved a higher drug release compared with the cubosome dispersion. The SEM micrograph of the selected sponge showed that it has an interwoven irregular fibrous lamellar structure with low density and high porosity. The *in-vivo* data revealed that topical application of the β-sitosterol cubosomal sponge showed significant higher wound closure percentage relative to the β-sitosterol product (Mebo)®.

Keywords β-sitosterol · burn · chitosan · composite sponge · cubosomes

Introduction

Natural medication like β-sitosterol are thought to prevent infection and speed up recovery without having any of the negative side effect of pure drugs. β-sitosterol, an angiogenic component derived from plants, has potential pharmacological applications in the therapy of chronic wounds as it stimulates epithelialization [1].

β-sitosterol functions by supplying moisture to the wound, which speeds up its regeneration and healing, fostering an environment that inhibits the growth of fungi and bacteria. It can generate an anti-inflammatory effect that reduces redness and swelling. In addition, it protects and isolates injured nerves surrounding the site of pain, thereby minimizing pain perception. However, it supplies wounds with the necessary nourishment, enhances residual heat absorption from burns, insulates the wound from external environmental damaging factors without impairing gas exchange and drainage, liquefies the necrotic tissue (dead tissue), lowers the loss of body fluids from burns, and facilitates quick cleaning and recovery of the affected skin area [2, 3].

Among lyotropic nonstructural carriers, cubosomes and hexosomes are the most studied. They are identified as colloidal nanoparticles that have 3D-well-organized bicontinuous cubic-phase internal structures [4]. The cubic form is considered one of the liquid crystalline phases that have received the most interest and have been extensively studied in the literature. It was observed that the inverse bicontinuous cubic phase's phase transition into the reverse hexagonal phase was accelerated by adding oleic acid at various concentrations [5]. The hexagonal shape of the cubosome closes the water channel and restricts the diffusion pathway more than the cubic phase. As a result, they gained more attention for their potential use as a diffusion-delaying matrix for the dissolved drugs [6, 7].

Classic hemostatic products such as bandages, gauze, and skimmed cotton are not the best choice for the hemostasis of

✉ Abeer Khattab
abeer_khattab75@yahoo.com

✉ Soha Ismail
sohaismail75@yahoo.com

[1] Pharmaceutics Department, Egyptian Drug Authority, Cairo Governorate, Egypt

[2] Physiology Department, Egyptian Drug Authority, Cairo Governorate, Egypt

deep injuries or irregularly penetrating wounds. In addition, an optimal burn wound dressing should promote faster tissue regeneration, shield damaged tissue from microbial invasion and have an appropriate fluid absorbance property [8]. Thus, the development of a novel type of hemostatic matrix with quick, safe, and effective properties, like composite sponge, is essential in case of an emergency involving burns [9–11]. The high porosity and hydrocolloid characteristics of sponges permit the diffusion of oxygen and maintain a moist environment at the wound bed, enhancing the wound healing efficiency of the developed matrix [12].

Hence, the aim of this research was to develop a β-sitosterol cubosomal sponge formulation (β-sito-cubs sponge) to improve the burn wound healing and to overcome the limitations of the conventional topical formulations. The wound healing efficiency of the developed formulation was determined by measuring the physical and histological changes observed at the wound bed. Further a comparable efficacy of the developed product was determined by comparing the wound healing efficacy of developed formulation with marketed formulation [12, 13].

Material

B-sitosterol, Tween 80 and 1-oleoyl-rac-glycerol (GMO) were supplied from Sigma-Aldrich, St. Louis, USA. Oleic acid (OA) and Hydroxypropyl methyl cellulose (HPMC) were obtained from Fisher Scientific UK, Loughborough, UK. Pluronic F127 (PF127) was obtained from Spectrum, Gardena, Canada. Methanol (HPLC grade), potassium dihydrogen orthophosphate, sodium chloride, potassium chloride, calcium chloride dehydrate, gelatin and glacial acetic acid were obtained from El-Nasr Chemical Co., Cairo, Egypt. Chitosan (Mwt 100,000-300,000) from ACROS Thermo scientific, USA.

Optimization of β-sitosterol Cubosomes Using Central Composite Design (CCD)

Using Design-Expert software® (version 7, Stat-Ease Inc., MN, USA), a CCD was performed to optimize the concentrations and characteristics of the cubosome and assess the effects of different variables. As the two independent variables, the concentrations of oleic acid (5 and 15%) and pluronic 127 (5 and 15%) were selected. The responses that were looked at were %EE, particle size (PS), and zeta potential (ZP). The concentration of β-sitosterol is maintained at 5 mg/ml in every formulation. The independent variables' levels are shown in Table I. Three center positions and the associated CCD-compliant formulations of different factor combinations are shown in Table II.

The Design Expert® software was utilized to assess the various responses through the application of the response surface analysis (RSA) and central composite model. An equation involving polynomials was used to express each response. Based on RSA of the collected data, the optimum formulation was determined by estimating the overall desirability. The desired optimized formula was targeted to have a minimum particle size (PS) and a maximum EE (%).

Table I Central Composite Design to Optimize Sitosterol Cubosomes

Independent variables levels (mg)	Low level	High level
Concentration of oleic acid (X_1)	5%	15%
Concentration of pluronic 127 (X_2)	5%	15%
Responses (dependent variables) EE%, PS, ZP		

Preparation of β-sitostrol Cubosomes According to Central Composite Design

The emulsification procedure, as described by Sherif *et al.* [13], was utilized to prepare β-sitosterol cubosomal dispersions. The lipid fraction was composed of GMO as a liquid-crystalline forming lipid, oleic acid (OA) as a phase convertor, and pluronic F127 (PF127) as a stabilizer. The lipid mixture was maintained at a constant 50 mg/mL. This mixture was melted in a thermostatic shaker at 70 °C, and then an amount of 100 mg β-sitosterol was completely dissolved in this molten mixture using a magnetic stirrer. A preheated aqueous solution (70 °C) was added dropwise to the molten mixture while being mechanically stirred for 15 minutes at 850 rpm. After that, the dispersion was homogenized for five minutes at 10,000 rpm. The developed formulae were stored at room temperature for further characterization.

Determination of Particle Size (PS), Polydispersity Index (PDI) and Zeta Potential (ZP)

The generated cubosomal dispersions' particle size, polydispersity index, and zeta potential were all assessed by Zetasizer (Nano ZS-90, Malvern Instruments, and UK). After diluting each sample (1:100) with deionized water, they were all subjected to two minutes of sonication. Every measurement was done three times for every sample, and expressed as average value ± SD.

Determination of the Drug Entrapment Efficiency EE (%)

A 2 mL aliquot of the cubosomal formula was rotated at 15000 rpm for one hour at 4 °C in a cooling centrifuge in order to ascertain the percentage of EE [3]. The amount of unentrapped B-sitosterol in the supernatant was measured after an appropriate dilution with methanol using a validated HPLC method. HPLC conditions are as follows:

Table II Composition and Characterization of Sitosterol Cubosomes According to CCD

Formula code	Concentration of pluronic 127 (%*)	Concentration of oleic acid (%) *	PS nm	%EE	ZP mV	PDI
F1	15	15	25.2±0.9	94.2±3.5	-48±1.5	0.474±0.01
F2	5	5	68.6±1.2	93.2±3.1	-18.3±1.9	0.325±0.05
F3	15	5	53.8±1.1	90.2±2.6	-28.3±2.4	0.354±0.04
F4	2.93	10	74.4±2.8	92.3±3.8	-29.6±1.1	0.367±0.02
F5	17.07	10	32.1±0.9	89.2±1.9	-43.7±1.8	0.368±0.02
F6	10	10	47.7±1.6	94.4±1.6	-36.4±2.2	0.375±0.01
F7	10	17.07	39.04±1.2	95.8±2.8	-45.5±1.7	0.368±0.05
F8	10	10	44.5±1.1	93.4±2.6	-35.6±1.9	0.356±0.04
F9	10	10	48.2±1.9	92.4±1.2	-34.7±2.6	0.374±0.02
F10	5	15	34.0±0.4	95.6±2.8	-43±2.3	0.358±0.07
F11	10	2.93	58.4±0.6	91.1±3.4	-23±1.7	0.478±0.06

*% w/w of the lipid fraction which was kept constant at 5% w/w in the all preparation

mobile phase (Methanol: water: acetonitrile (87.5:10:2.5)), λ max 205 nm, injection volume of 50µl, flow rate of 2µl/min using column C8: 4.6 x 250 mmx 5µm) The findings were reported as mean values with a standard deviation (SD) after the experiment was conducted three times. The following formula is used to determine EE%.

$$EE\ \% = \frac{\text{Total amount of drug} - \text{Amount of un} - \text{entrapped drug} \times 100}{\text{Total amount of drug}} \quad (1)$$

Morphological Examination of Cubosomes

Transition electron microscopy (TEM) was used to study the morphology of the optimized formula in order to verify the polygonal structure of the produced cubosomes. The negative staining method was carried out using 2% w/v phosphotungistic acid. A single drop of the diluted cubosomal dispersion was put to a copper grid that had been carbon-coated before staining. After allowing the material to cure at room temperature, a TEM examination was performed.

Preparation of β-sitosterol Cubosome Sponge

Firstly, 1% w/v of chitosan (in 1% glacial acetic acid), 1% w/v of gelatin (in distilled water), and 1% w/v of HPMC (in distilled water) were prepared. As shown in Table III, An aliquot of 5 ml of chitosan solution was mixed very well with 5 ml of each polymer solution (gelatin or HPMC) using a magnetic stirrer. Then, tween 80 (1.5% w/v of the total volume) was added to the polymer solution mix. An aliquot of the optimized cubosomal dispersion was added to the mixture to obtain a final concentration of β-sitosterol equivalent to 0.5 mg/mL. After that, all blends were homogenized until opaque aqueous mixtures were obtained. The mixtures were sonicated for 15 minutes to remove any air bubbles. To obtain the sponge, each formulation was transferred into a petri dish of 3 cm in diameter, frozen over night at -80 C, and then freeze dried at -35 C for 48 hours in a freeze dryer (Snijders Scientific, Holland) [14].

Table III Composition of Prepared β-sitosterol Cubosome Sponge (β-sito-cubs Sponge)

Formula code	Chitosan solution (1% w/v)	Gelatin Solution (1%w/v)	HPMC solution (1%w/v)	Tween 80
SP1	5 ml	5 ml	-	-
SP2	5 ml	5 ml		1.5%
SP3	5 ml		5 ml	-
SP4	5 ml	-	5 ml	1.5%

Characterization of β-sitosterol Cubosome Sponge

Density, Porosity and Water Absorption Capacity

By determining the sample's weight and geometric measurements at least three times, the density of the sponge was computed. The porosity was determined using the technique described by Fan *et al*. [12]. In brief, the sponge's initial weight was identified as W_0. The sponge was then submerged in dehydrated alcohol at room temperature for a whole day. After gently removing the ethanol from the surface with filter paper, the weight of sponge that was saturated with dehydrated alcohol, was measured and the weight was recorded as W_t [15, 16]. Equation (2) was utilized to determine the porosity of the sponges.

$$P = W_t - W_0/\rho_0\, V_0 \times 100 \quad (2)$$

Where P is the porosity, W_0 is the original weight of the sponge, W_t is the weight of the ethanol-saturated sponge, V_0

is the original volume of the sponge, and ρ_0 is the density of the dehydrated alcohol (0.79 g/mL).

To estimate the water absorption capability of the sponge, each sponge formula was weighed (W_1), then immersed in 50 mL of water. The fully hydrated sponges were removed and held until no water dropped [15, 16]. The water absorption capacity of sponges was determined using Eq. (3):

$$\text{Water absorption} = W_2 - W_1/W_1 \quad (3)$$

where W_2 and W_1 refer to the weight of fully hydrated and dry sponges, respectively.

Cyclic Squeezing-absorbing Water Property

It was assessed how well sponges absorbed water through the cyclic squeezing-absorbing technique. Samples of sponges were hydrated in water and then squeezed to extract the absorbed water by hand-pressing them between filter papers. The filter paper was changed until there was no more discernible water on the filter paper'. The procedure was then repeated [12]. Equation (3) above was used to estimate the cyclic squeezing-absorbing water capacity.

Measurement of the Sponges Mucoadhesion

TA-XT Plus Texture Analyzer was used in conjunction with an appropriate mucoadhesive holding probe to carry out the mucoadhesion test. Using cyanoacrylate adhesive, a mucin tablet was attached to the apparatus's base while the sponge sample was secured to the upper probe of the device. After wetting the sponge with 100 µl of PBS, it was left in contact with the mucin tablet. A weight of 5 g contact force was applied and held for 20 seconds. The probe was then raised at a speed of 0.1 mm/sec, and the detachment force was measured until the sponge and mucin tablet were totally separated [14].

In-vitro Release Study

The medication release was evaluated using the modified USP dissolution equipment 5 [17] for transdermal formulation. Every sponge formula (5 milligrams of β-sitosterol) was placed on a watch glass and covered by a plastic screen. The sponge-filled watch glass was inserted into the vessel. Each vessel held 250 milliliters of phosphate buffered saline (PBS) with a pH of 7.4, was maintained at 37°C ± 0.5, and spun at 50 ± 0.2 revolutions per minute [18]. PBS was prepared using 8 g of NaCl, 2.2 g of KCl, 1.44 g of Na2HPO4, and 0.245 g of KH2PO4 in 1000 ml of distilled water, and the pH was adjusted to 7.4. Three milliliters of the sample were removed from the release medium at various intervals (15, 30, 60, 120, 180, 240, and 360 min) and replaced with an equivalent amount of freshly prepared buffer solution kept at 37°C. The previously described HPLC method was used to determine the drug released from various formulations. Following each sampling, a correction factor was applied. In parallel, the dissolution of the lyophilized optimized cubosome formula (equivalent to 2.5 mg β-sitosterol) was also carried out for comparison. To study the kinetics and mechanism of the drug release from different cubosome sponge formulae, the data obtained from the drug release study were fitted to different kinetic models; zero order, first order, Higuchi and Krosmeyer-peppas equation, and the highest r^2 and n (diffusional exponent of krosmeyer equation) were determined.

In Vivo Study

Experimental Groups and Burn Model

Twenty-four male albino rats, weighing 250-350 g, were used for the current study. The rats were kept in appropriate separate cages, at an average temperature of 24 °C, and 12 hours of darkness and 12 hours of light were provided. The rats were divided into four groups, and each group 6 rats were treated as follows: Control group (gp1), Sham group (Untreated group, gp 2), β-sitosterol cubosomes sponge (β-sito-cubs sponge, gp3) group and β-sitosterol cream group (Mebo® marketed product, gp 4).

All rats were anesthetized with ketamine (10 mg/kg) in addition to xylazine (80 mg/kg) intraperitoneal injection. The hair at the dorsal region was shaved and cleansed with alcohol swab. Second-degree burn wound was inflicted using iron plate measuring 2×2 cm which was warmed in boiling water for 5 minutes and placed for 30 seconds on the shaved area. For treated groups (gp 3 and 4), an amount of Mebo cream and cubosome sponge equivalent to 2.5 mg of β-sitosterol were topically applied to the burned area once a day for 14 days. The rats were kept in separate cages to prevent the rats from harming each other after burn model induction. At the end of the experiment, all rats were anesthetized by injecting ketamine (10 mg/kg) and xy lazine (80 mg/kg) Intraperitoneally. The rats were euthanized by cervical dislocation, and the injured tissues were carefully dissected and stored for biochemical and histological examination [18]. All the animal experimental protocols were approved by the Institutional Animal Ethics Committee (IAEC), National Organization for Drug Control and Research, Egypt.

Macroscopic Examination and Wound Closure Percentage

A macroscopic examination of the burned area for all groups was done and the wound closure percentage was determined

after 7 days and 14 days by measuring the burned area according to equation [19]:

$$BCA = \{(BCA\ day_0 - BCA\ day_x)/BCA\ day_0\} \times 100 \quad (4)$$

BCA : Burn closure area

$BCA\ day_0$: primary wound area and $BCA\ day_x$: wound area at X day

Oxidative Stress Parameters

The previously prepared homogenates from skin tissues were used to measure malondialdehyde (MDA) level as described formally by Karatepe *et al* [20]. The level of Glutathione (GSH) [21] and Superoxide dismutase (SOD) were evaluated using assay kits from Biodiagnostic, Egypt, according to the manufacturer's protocols.

Histopathological Examination

For histological study, Formalin-fixed sections of skin tissues from each group were embedded in paraffin, cut by microtome into 4-5 µm thickness and stained with hematoxylin and eosin (H&E) and Masson. The stained sections were examined using light microscopy (U-III Multi-point Sensor System; Nikon, Tokyo, Japan).

Statistical Analysis

All data were represented as mean ± S.E. and subjected to statistical analysis using Statistical Package Software System version 25. Significant differences among means were evaluated using one-way ANOVA followed by Duncan posthoc test. Probability of less than 0.05 was considered significant.

Results and Discussion

Formulation and Optimization of β-sitosterol Cubosomes

Eleven preparations with three central points were prepared as demonstrated in Table II. The obtained results were subjected to ANOVA analysis followed by the calculation of desirability values to obtain the optimized formula.

Determination of Particle Size (PS), Polydispersity Index (PDI) and Zeta Potential (ZP) of Cubosomal Dispersions

Table II showed the range of particle sizes for the formulations, which were between 25.2 and 74.4 nm. PS values were analyzed by ANOVA using a linear model (p-value = 0.0008). The model showed a non-significant lack of model fit (p-value 0.0657), which indicates the validity of the model. In addition, the adequate precision value was 12.383, which indicates the signal-to-noise ratio is better than 4. The results revealed a significant effect of PF127 and oleic acid, with p-values of 0.0014 and 0.0032, respectively. In terms of coded factors, the final equation that represents the correlation between PS and the two responses was:

$$PS = +47.55 - 9.9X_1 - 11.33X_2 \quad (5)$$

It was clear from Fig. 1 that the increase of both oleic acid and PF127 led to a significant decrease in PS values. These findings were in accordance with the results attained by Zhang *et al*. and Nakano *et al*. [22, 23], who observed the profile of PS against the percentage of oleic acid in the lipid fraction, and this was justified presumably because the initial decrease in PS with increasing oleic acid percent up to 40% is most probably due to the decrease in the hydrophobicity of the lipid core owing to the negatively charged oleic acid; but with the further increase of oleic acid above 40%, the non-charged oleic acid moiety predominates, leading to an increase in the hydrophobicity and consequently an increase in the PS.

PDI values varied from 0.325 to 0.478 (Table II) and all were less than 1 which indicated good size distribution and less chance for agglomeration [4]. Previous research addressed the effect of particle size and PDI on the cell uptake of nanocarrier system. It was reported that the particle size and PDI of nanocarrier systems are the main physicochemical attributes that influence the endocytosis-dependent cellar uptake and the tendency of them to accumulate in the target tissue. Moreover, the particle size of lipidic vesicles has been shown to have a significant influence on bioactive delivery into the skin. Nanovesicles with a diameter of 300 nm or below are able to deliver their contents to some extent into the deeper skin layers. Nanovesicles with a diameter of 70 nm or below, have shown maximum deposition of content in both viable dermal and epidermal layers. while those with a particle size of below 36 nm can be absorbed through the aqueous pores. In general, particles in the size range of 10–210 nm, however, may preferentially penetrate through the transfollicular route [24, 25]. PDI is used to describe the degree of non-uniformity of a size distribution of particles. The successful formulation of safe, stable and efficient properties, requires the preparation of homogenous (monodisperse) populations of nanocarriers of a certain size [24, 25]. This index is dimensionless and scaled such that values smaller than 0.05 are mainly seen with highly monodisperse standards. PDI values bigger than 0.7 indicate that the sample has a very broad particle size distribution (82). a PDI of 0.3 and below is considered to be acceptable and indicates a homogenous population of

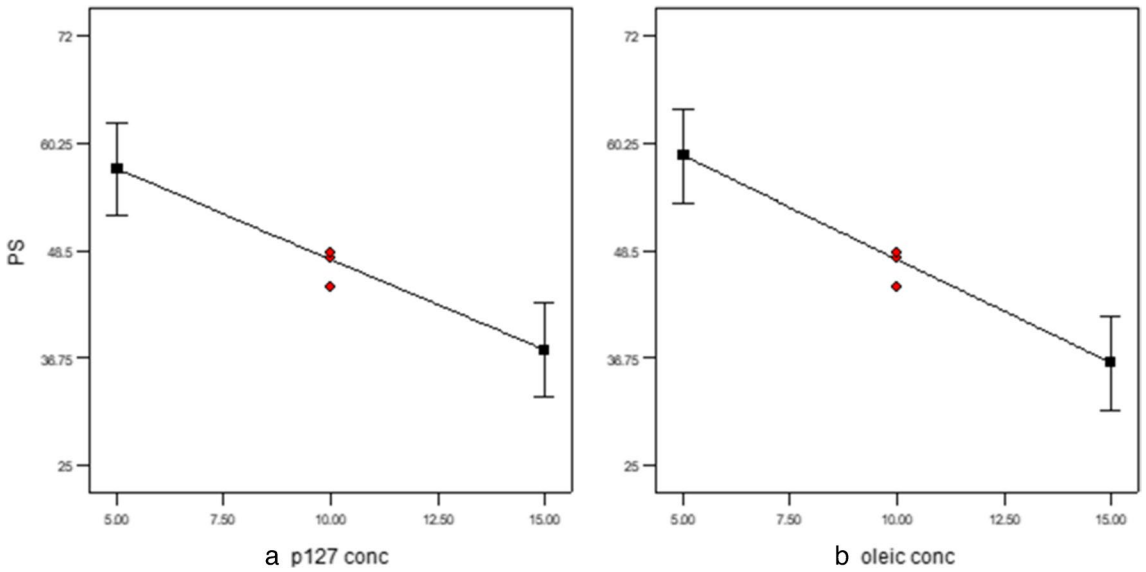

Fig. 1 Main effect of oleic acid (**a**) and pluronic F127 (**b**) on Particle size of cubosomes

phospholipid vesicles [24]. Although the last edition of the FDA's "Guidance for Industry" concerning liposome drug products emphasizes the importance of size and size distribution as "critical quality attributes (CQAs)", as well as essential components of stability studies of these products, it does not mention the criteria for an acceptable PDI [26]. Every developed formulation had a PDI of less than 0.5 and an appropriate particle size, both of which suggested that they would be good for skin delivery.

All ZP values ranged from -18.3 (F2) to -48 (F1) mV. It is noted that most of the cubosomal formulas have ZP values above -30 mV, which is well known as a highly stable dispersion [4]. Response surface analysis of the obtained ZP values utilizes the suggested quadratic model (p-value = 0.0007). The ANOVA analysis showed a nonsignificant lack of model fit (p-value 0.0808). A significant effect of the two variables, oleic acid and PF127, with p-values ˂ 0.0001 and 0.003, respectively, was observed. As shown in Fig. 2, it was observed that the increase of both oleic and pluronic F127 led to an increase in ZP values. In addition, the adequate precision value was 16.349. The "Pred R-Squared" of 0.9712 is in rational agreement with the "Adj R-Squared" of 0.9423. The final equation to correlate the two responses and ZP in terms of coded factors was

$$\begin{aligned} ZP &= -35.57 - 9.53X_1 - 4.37X_2 + 1.25X_1X_2 \\ &\quad + 0.92\,X_1^2 - 0.28\,X_2^2 \end{aligned} \tag{6}$$

Determination of the Drug Entrapment Efficiency EE %

Table II showed effective entrapment of β-sitosterol, with EE percentages ranging from 89.2% to 95.8%. The results were subjected to ANOVA analysis utilizing the quadratic model with a p-value of 0.0189. In addition, the lack of fit of this model was nonsignificant with a p-value of 0.5459. The analysis showed the significant effect of changing the percentage of both oleic acid and PF127, with p-values of 0.0055 and 0.0256, respectively. The generated equation for the EE (%) analysis was:

$$\begin{aligned} EE\ (\%) &= +91.13 - 0.094X_1 + 0.44X_2 \\ &\quad + 0.016X_1X_2 + 0.013X_1^2 - 0.041X_2^2 \end{aligned} \tag{7}$$

As seen in Fig. 3, there was a notable rise in the EE (%) of β-sitosterol when the proportion of oleic acid was increased. This could be explained by the direct relationship between the lipid core's hydrophobicity and oleic acid percentage. However, the inclusion of a liquid phase in the formulation has been verified to offer enough space for the drug particles to be arranged within the system's porous network, resulting in an enhanced DEE% [27]. On the other hand, DEE% decreased with increasing PF127%, and that could be attributed to PF127's solubilization effect for β-sitosterol in the aqueous phase [28].

Optimization of β-sitosterol Cubosome Formulations

The selection of the optimized formula was done using desirability calculations. The goal was to develop an optimized formula with the lowest PS and the maximum EE (%). Formula F10, which showed the highest desirability of 0.852, was selected for further study. Figures 4 and 5 showed the PS distribution and zeta potential curves of the optimized formula, respectively.

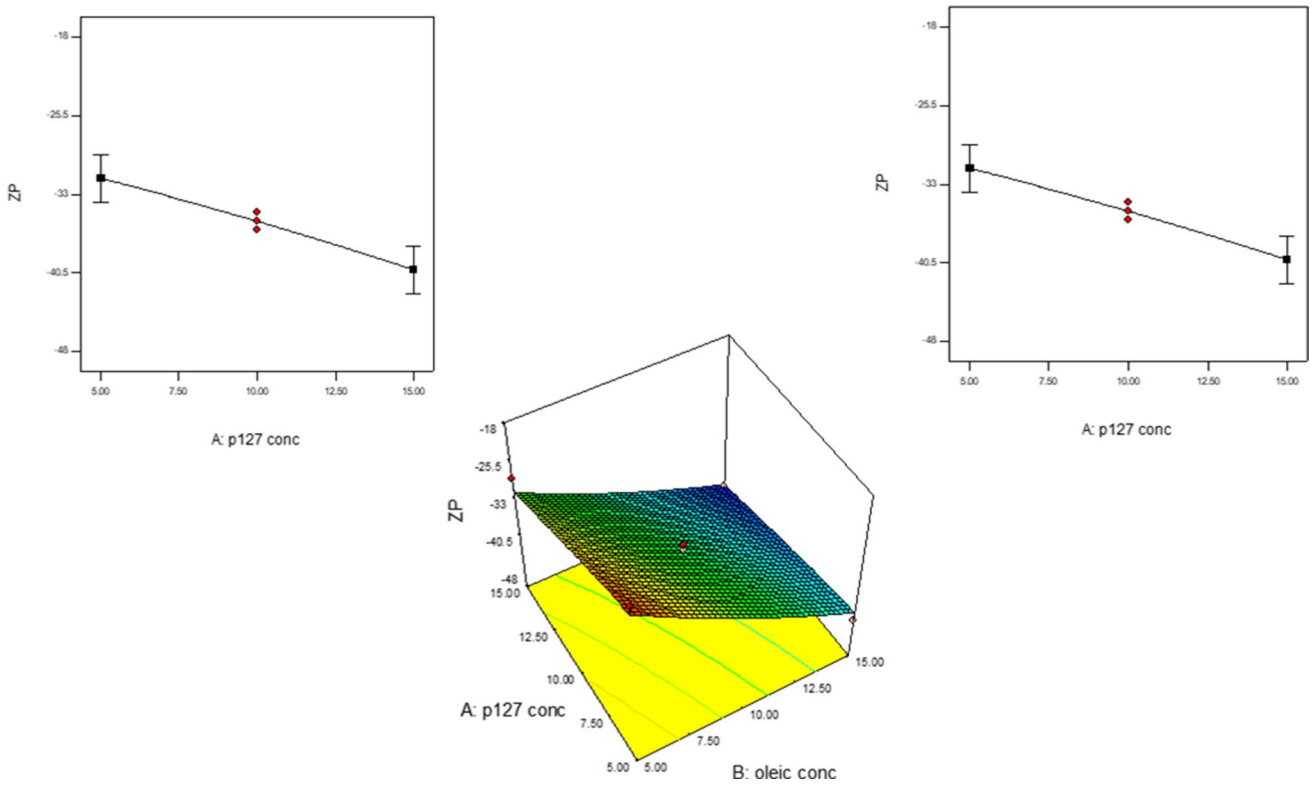

Fig. 2 Main effect of oleic acid (**a**) and pluronic F127 (**b**) on Zeta potenial of cubosomes

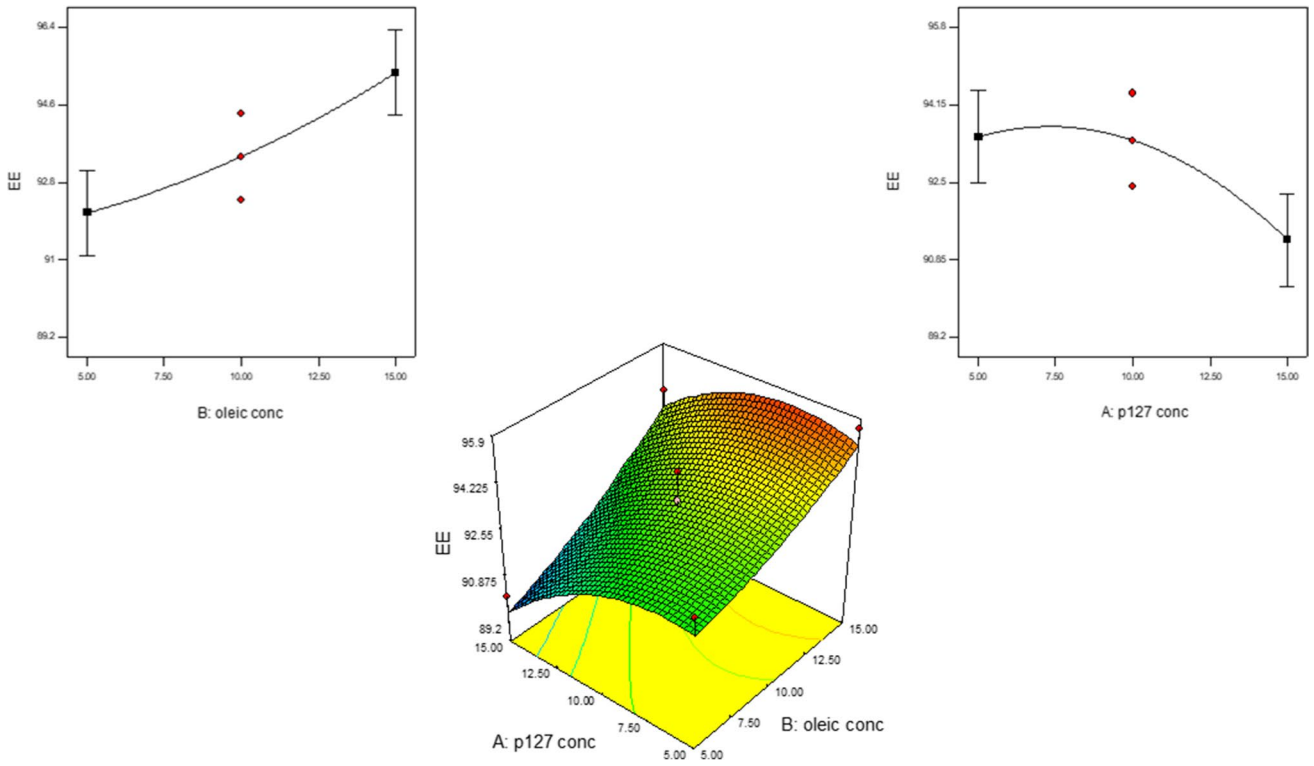

Fig. 3 Main Effect of Oleic Acid (**a**) and Pluronic F127 (**b**) on EE% of Cubosomes

Morphological Examination of the Optimized Cubosome Formulation

Morphological examination by TEM confirmed the hexagonal structure with uniform size of the optimized cubosomal dispersion (Fig. 6). The particles were well separated, and no aggregation was observed. The particles were in the nanosize and that matched the PS analysis results.

Characterization of Sponges

Density, Porosity and Water Absorption Capacity

The density of the sponge formulations ranged from 22.4 to 28.5 g/cm3, as shown in Table IV. The results showed that formulations having Tween 80 had higher porosity and higher absorption capacity than formulations without. The high-water absorption capacity and rapid water absorption rate are crucial for rapid hemostasis in deep wounds. The high porosity and fluffy nature of the formulations might be attributed to the increased bubble formation in the polymer solution. The presence of surfactant helps render sponges more porous and fluffier, which in turn helps improve their water absorption capacity. After the first squeeze, the water absorption capacity of sponges containing the surfactant changed obviously. This might be due to the collapse of the partial pore construction during the pressing, resulting in a significant decrease in water absorption capacity. After being squeezed three times, the pore structure of sponges has substantially reached balance, and the water absorption capacity no longer changes with further squeeze [12]. Although the water absorption capacity is reduced to some extent, the sponges containing surfactant could still reabsorb water instantaneously and recover their original size and shape compared with sponges without Tween 80. It could be concluded that the water absorption capacity and shape recovery of the sponge depend on its porosity and microstructure.

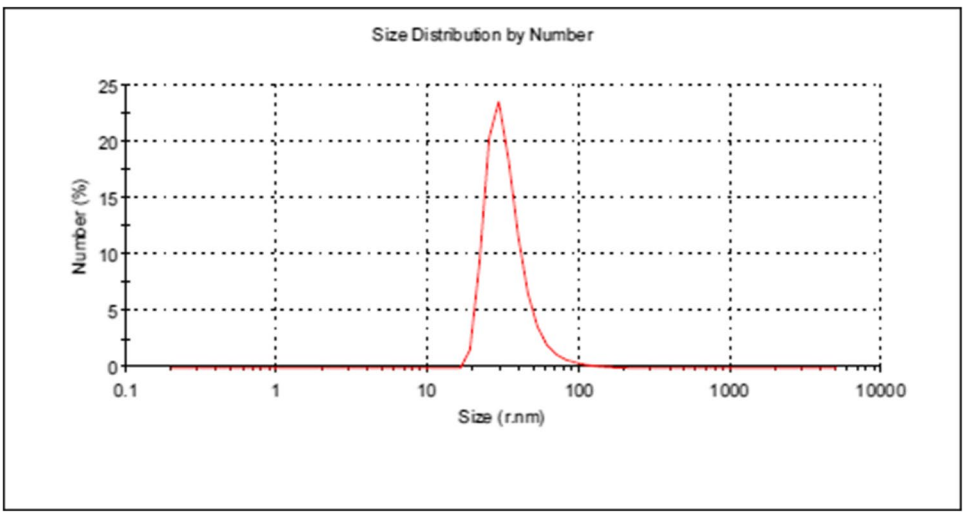

Fig. 4 Particle size of the cubosomal optimized formula (F12)

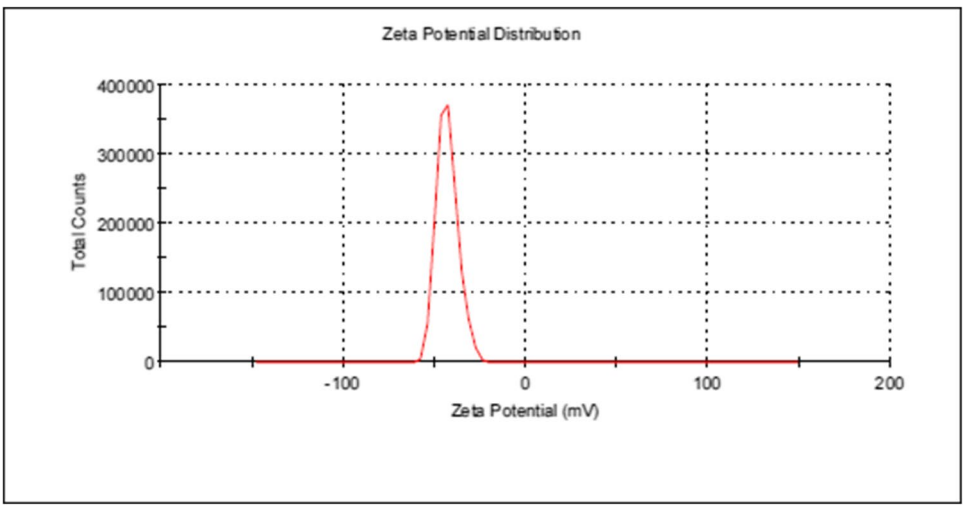

Fig. 5 Zeta potential of the cubosomal optimized formula (F12)

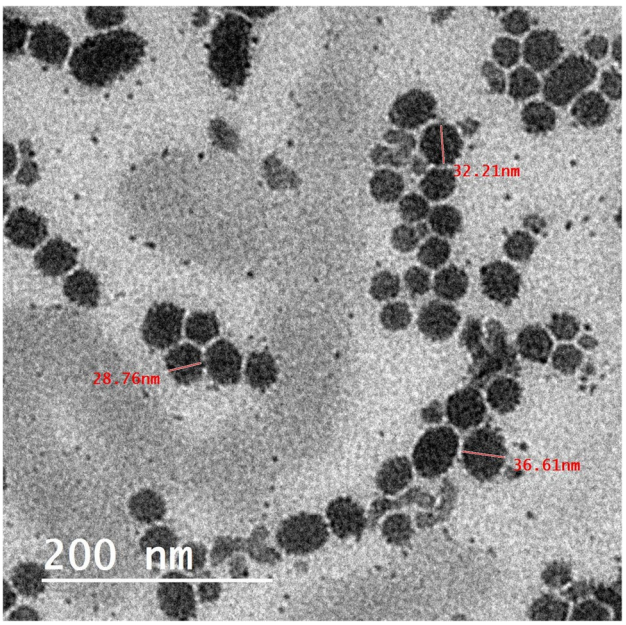

Fig. 6 TEM micrographs of the cubosomal optimized formula (F12)

Table IV Characterization of β-sitosterol Cubosome Sponges (β-sito-cubs Sponge)

Formula code	Density mg/cm^3	Porosity%	Absorption capacity (mg/mg)	Mucoadhesion (N)
SP1	22.4	76.9	14.6	1.7
SP2	23.5	79.6	15.3	1.2
SP3	27.6	80.5	16.4	2.0
SP4	28.5	88.7	17.94	2.3

The results of mucoadhesion force indicated that formulations having HPMC revealed higher adhesion forces than those that containing gelatin. The fibers and lamellar of the composite sponge are closely connected to maintain a good pore structure, which is favorable for adhesion. Therefore, formula SP4 was selected for the *in vivo* study.

In-vitro Release Study

In vitro drug release profiles up to 12 h from the four cubosomal sponges (β-sito-cubs sponge) compared with the lyophilized optimized formula (F10), were illustrated in Fig. 7. The percentage release of β-sitosterol from F10, SP1, SP2, SP3 and SP4 were 67.6%, 39.3, 90.2, 55.5 and 92.5 %, respectively. This low drug release % from F10, SP1 and SP3 might be due to the structure characteristics of the formed cubosomal liquid crystalline particles which led to drug diffusion firstly from the lipophilic particle to the surrounding aqueous medium. On other hand, the high drug release from SP2 and SP4 may be due to the influence of Tween 80 as solubilizing agent. The kinetic mechanism of the drug release from the different sponge formulae and the optimized cubosome formulation revealed diffusion mechanism. The results revealed that formulae SP1 and SP3 showed a non-Fickian mechanism (anomalous transport) in which the release of the drug is controlled by the swelling of the sponge matrix and the rate of polymer relaxation is near to the rate of drug diffusion. On the other hand, formulae SP2 and SP4 that contain Tween 80 showed a Fickian mechanism, since the presence of Tween 80 may increase the porosity of the sponge matrix and the surface area of drug diffusion. Therefore, there is no boundaries between the swollen polymeric matrix and the dry polymeric matrix, and the rate of the polymer relaxation is about the same as the rate of water diffusion.

Morphology

SEM micrograph of the selected sponge (SP4) presented in Fig. 8 showed that the sponge has an interwoven irregular fibrous lamellar structure with low density and is fluffy. The drug cubosomal particles were detected in the lamella and within layers of the sponge. It was clear that there was drug distribution throughout the porous sponge structure. Tween 80 is able to form many hydrogen bonds with polymer chains, which helps to separate the fiber bundle and promote the fluffier structure of sponge.

In Vivo Study

Burns are considered as one of the most serious skin injuries. The goal of burn care and therapy is rapid healing and epithelization to avoid infection. Topical therapy reduces the risk of burn wound infection in patients with serious burns, which is crucial for their survival [18]. Thermal burn injuries have 3 categories: scalds, contact burns, and fire. Contact burns are caused by touching hot surfaces that exhibit direct heat-induced protein denaturation and cell death (necrosis and apoptosis), which based on inducing free radical-mediated injuries and delayed tissue repair outcomes [29]. Moreover, the conversion of burn wounds to full-thickness burn could cause more severe consequences, such as systemic inflammation, local infection and even sepsis, which lead to a poor prognosis and great risk of mortality [30].

β-sitosterol is one of the most common plant-derived steroids with a structure similar to that of cholesterol. It was previously reported that β-sitosterol has anti-inflammatory and antioxidant and antimicrobial effects [31].

The macroscopic examination revealed the overall look and the rate at which the deep partial-thickness wound contracted during the healing process [32] in the skin of male

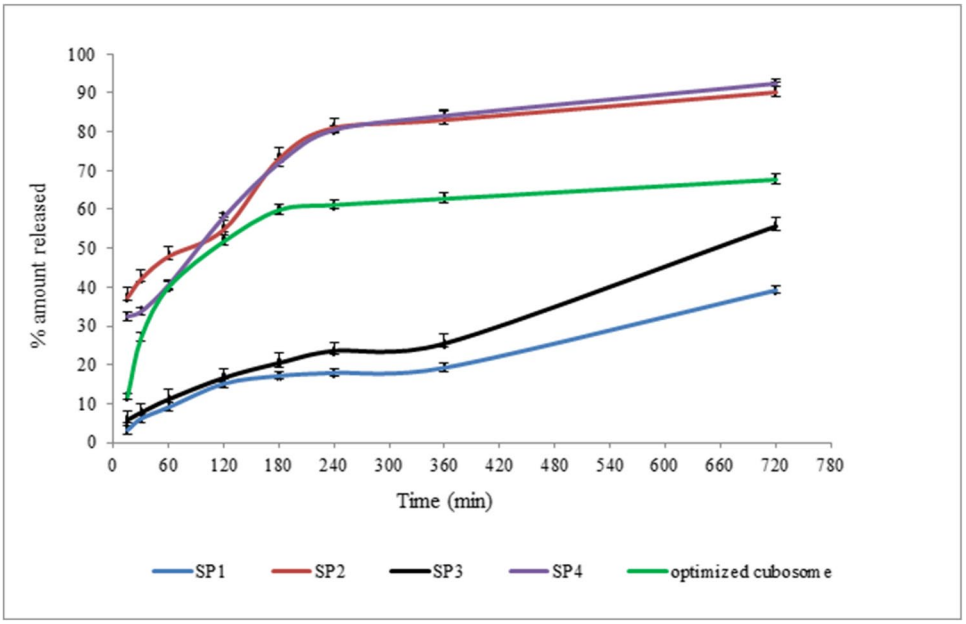

Fig. 7 *In-vitro* release from the four cubosomal based sponge (SP) compared with the lyophilized optimized formula

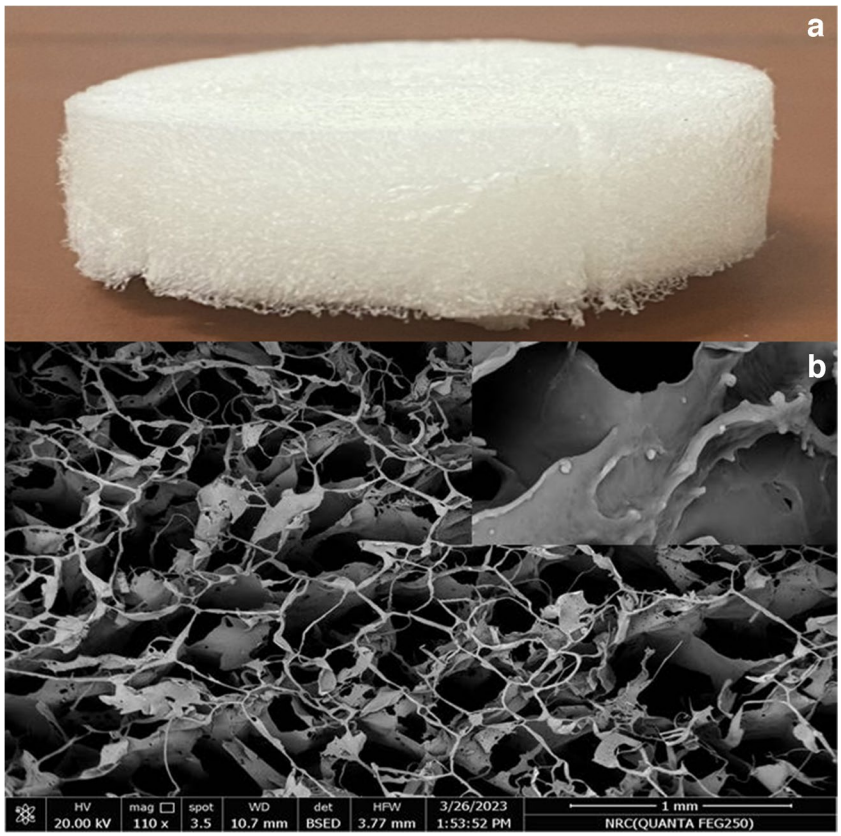

Fig. 8 Morphological structure of cubosomal sponges (**a**), SEM micrograph shows the porous interwoven fiber network structure of the optimized sponge showing the imbedded drug in the sponge structure (**b**)

albino rats after treating with Mebo® and β-sito-cubs sponge (SP4) following induced thermal burn. Figure 9a showed the macroscopic photos of burn areas after day 7 and 14 days compared to zero day. Severe edema was observed after burn process, forming marked white wounds. There were no blister and bubbles observed on the burn area. Also, there were no edges between the wound area and the normal skin. From 0 day to the 7th day of burning process, the white burn area damaged the skin barrier and hyperemia occurred into damaged tissue area of all groups. This hyperemic zone indicated the presence of red blood cells under extravasation. Then the formed scare shrank in size and turned dark

in all treated groups. The scare of β-sito-cubs sponge treated group was darker and slightly smaller than the other groups ($p>0.05$). On the 14th day, the wound area become smaller in all groups. the scare was still found in sham group and epithelialization process had not yet achieved. The scare was detached in Mebo and β-sito-cubs sponge groups, while epithelialization began only in β-sito-cubs sponge treated group.

The wound closure percentage after 7 and 14 days during the recovery phase is presented in Fig. 9b. There was a non-significant decrease in the size of the burn areas among all groups after one week compared to zero day. After 14 days, the Sham group showed moderate burn reduction percentage, while Mebo® and β-sito-cubs sponge groups showed a remarkable increase in the wound healing in terms of the reduction of percentage burn area. In addition, the cubs-β-sitosterol group showed significant reduction in wound area compared to Mebo® group.

Throughout the healing process, the wound always contracted; however, the rate of contraction only significantly increased in the 15th day following the burn. According to earlier study, the fibroblasts that migrate towards the wound borders could generate enough force to start the constriction of the wound. Further contraction of the wound was facilitated by the actin cytoskeleton, as migratory fibroblasts differentiated into myofibroblasts as the contraction progressed. Additionally, at the late stage of recovery, the fibroblasts production always increased [32]. As a result, the late stage of healing showed the obvious wound contraction.

Burn wound healing is a complicated physiological process through which damaged skin tissue regains the normal anatomy after thermal injury [33]. During the healing process, keratinocytes and epidermal cells from wound edges proliferate inward and contract the wound size. Wounded area contains reactive oxygen species which give rise to oxidative stress leading to lipid peroxidation, DNA damaging, and enzyme inhibition or inactivation, including free-radical scavenger enzymes [34]. Therapeutic strategies that target reactive oxygen species depletion during wound treatment may reduce inflammation and facilitate the transition from the inflammatory to proliferative phase. Many reported evidences suggest antioxidants of natural origin such as plant flavonoids are capable of reducing the oxidation of cellular molecules by stopping free radical chain reaction or by a scavenging of reactive oxygen species [1]. B-sitosterol accelerates wound healing process through multiple mechanisms

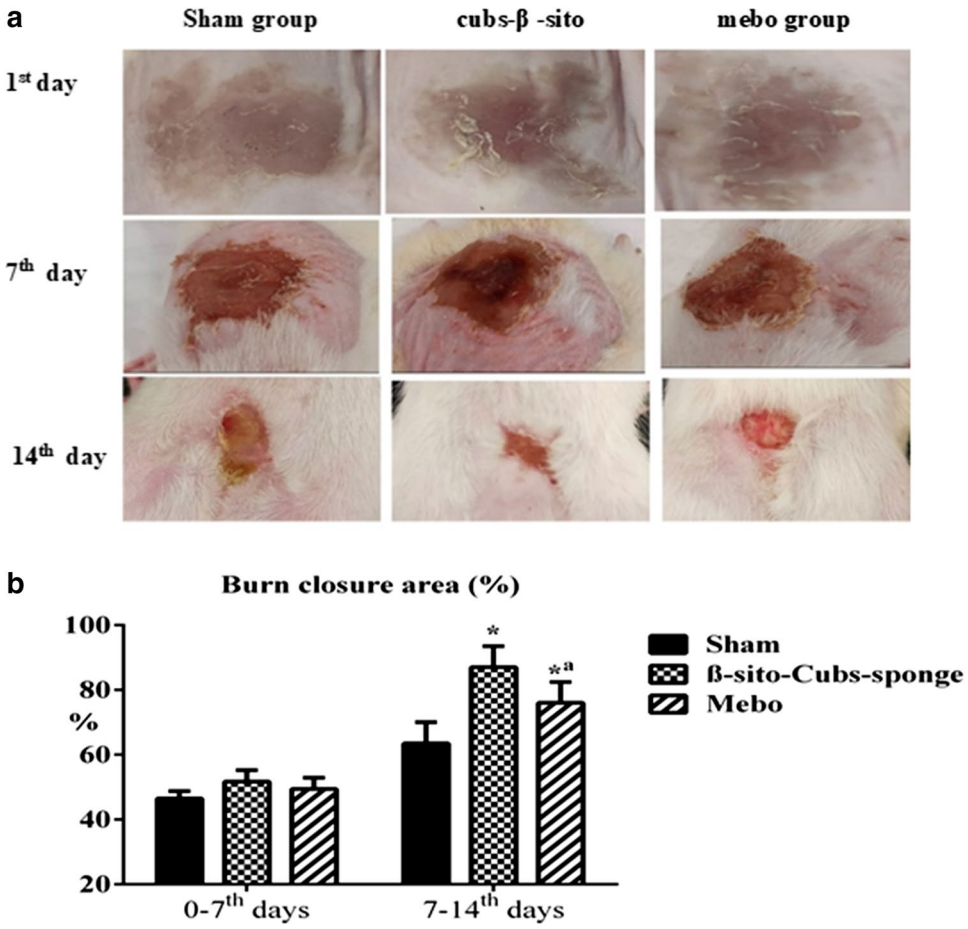

Fig. 9 **a** Macroscopic photos for the full-thickness dermal burned area in sham, Mebo and β-sito-cubs sponge groups, showed the progress of healing after 7 and 14 days compared to zero day. **b** The effect of β-sito-cubs sponge on wound closure percentage after 7 and 14 days compared to zero day. *p: significant difference from control group within the same time interval ($P < 0.05$). [a]p: significant difference between mebo and the β-sito-cubs sponge groups with in the same interval ($P < 0.05$)

such as upregulating various growth factors, cell division, maturation and migration of various cells participated healing process. However, it may be suggested that keratinocytes, epidermal cells and fibroblasts were activated by the β-sitosterol to accelerate the healing process. On the other hand, β-sitosterol increased SOD activity and GSH significantly. Some wound healing agents have the ability to prevent oxidative damage and promote the healing of wounds on the skin by upregulating the production of antioxidant enzymes such as SOD and GSH [1]. The data reported in Fig. 10a, b showed a significant (P<0.05) decrease in GSH and SOD contents in sham group as compared to control group. groups treated with either Mebo or β-sito-cubs sponge exhibited a considerable (P<0.05) increase in both GSH and SOD content as compared to the sham group. Moreover, a negligible difference between the two treated groups in GSH levels was observed. These results were in agreement with previous studies [34, 35].

The data presented in Fig. 10c demonstrated that, in comparison to the control group, the sham group exhibited a substantial rise in MDA level (P<0.05). In contrast to the sham group, treatment with Mebo or β-sito-cubs sponge resulted in a considerable decrease in the elevated MDA levels. Apart from the group treated with β-sito-cubs sponge exhibited a more significant impact. This magnification effect of β-sito-cubs sponge rather than Mebo could be attributed to the nano-size of cubosomal formulation that increase permeability of β-sitosterol. Moreover, the mechanism of the cellulose-chitosan sponge mostly comprises the subsequent aspects. The sponge absorbed some water from the burn bed relying on its strong water absorption capacity. In addition, the chitosan can promote the aggregation of platelets and red blood cells to form thrombus. Moreover, the compressed hemostatic sponge swells rapidly after imbibing fluid, and forms a certain compression force on the wound by relying on its rapid shape recovery ability after absorbing water [12].

Masson staining Fig. 11a, b, c was a good indicator of burn wound depth. The red dye intensity reveals the tissue necrosis boundary. The intensity of this dye in sham group was distinctly higher than that in Mebo group than that of β-sito-cubs sponge group, indicating delaying in healing process in sham and Mebo group more than that of β-sito-cubs sponge group. Fewer residual cutaneous appendages and more severe

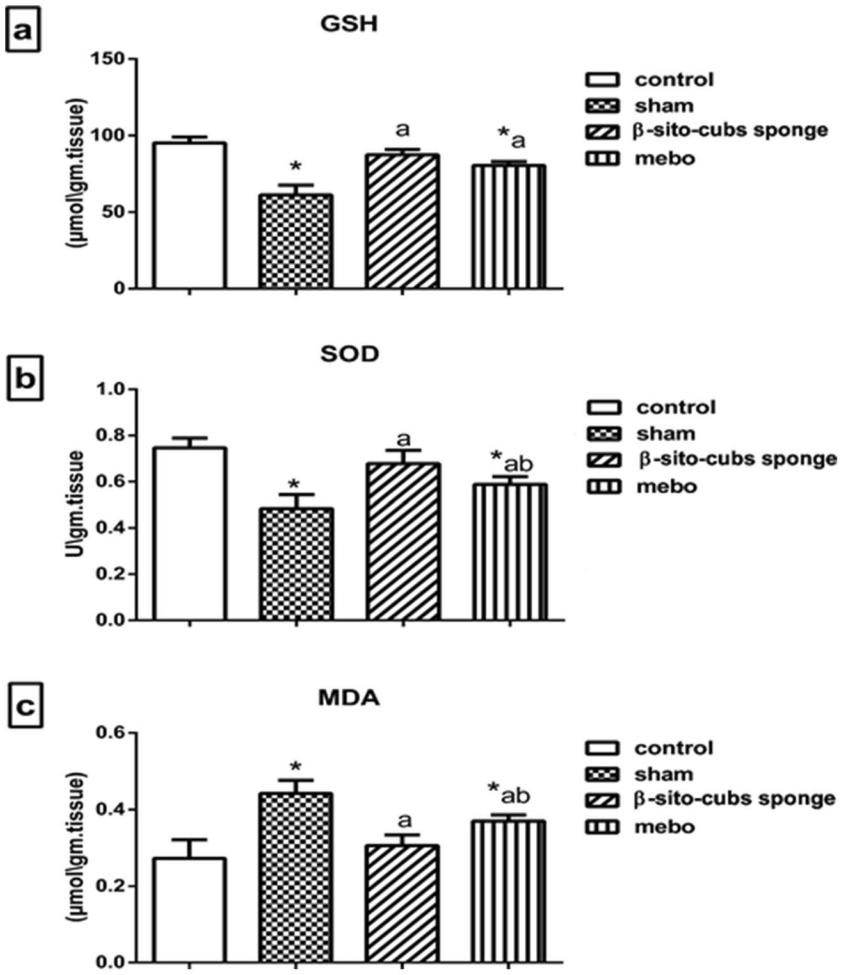

Fig. 10 **a**, **b**, **c** The effect of β-sito-cubs sponge on dermal antioxidants (GSH & SOD) and free radicals (MDA). *p: significant difference from control group (P < 0.05). [a]p: significant difference between sham group and the treated group (P < 0.05). [b]p: significant difference between β-sito-cubs sponge and Mebo group (P < 0.05) within the same column

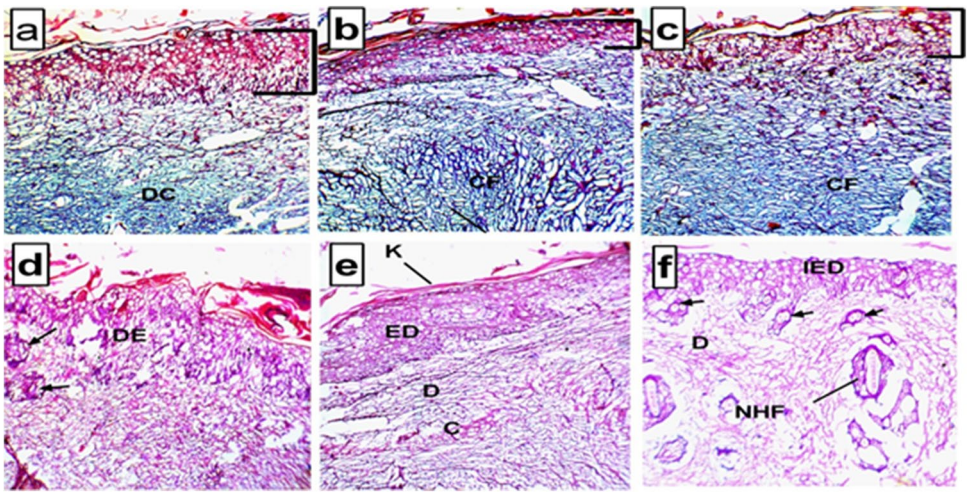

Fig. 11 Histological features of wound healing in rats. Images of skin tissue sections stained with Masson (a, b, c) for indicating the depth of burn wound, (**a**) skin section of sham group showing large inflamed and necrotic area, in addition to denaturation collagen fibers (DC). (**b**) skin section of β-sito-cubs sponge group showed improve of wound with decrease of inflamed region, and normal organization of collagen fibers (CF). (**c**) skin section of Mebo group showed moderate inflamed area and normal organization of collagen fibers (CF). Images of skin tissue sections stained with H&E, (d, e, f) showing histological changes during the wound-healing process in all experimental groups. (**d**) skin section of sham group showed disturbed constructions of epidermis layer (DE), and degenerated hair follicles (arrow). (**e**) skin section of β-sito-cubs sponge group showed complete epidermis layer (ED), apparent intact keratin lamellae (K) as well as an intact dermal layer (D) and collagen layer (C). (**f**) skin section of Mebo group showed incomplete epidermis layer (IED), neo hair follicle (NHF), while degenerated hair follicles (arrow) still found

collagen denaturation were seen at sham while β-sito-cubs sponge and Mebo groups showed organized collagen fibers.

Figure 11d of skin section of sham group stained with H&E showed disturbed constructions and thickening of the epidermis layer and degenerated hair follicles. on the other hand, Fig. 11e for β-sito-cubs sponge group showed complete mature epidermis layer with apparent intact keratin lamellae, an intact dermal layer and more organized collagen layer. However, skin section of Mebo group Fig. 11f showed incomplete epidermis layer, and neo formed hair follicle.

Conclusion

The formulation of β-sitosterol cubosomal nanoparticles with nanosize, high negative charge, and high EE% was successfully optimized using a central composite surface analysis. Not only that, but it could successfully maintain a controlled release over 12h. A simple and efficient dressing of porous and hydrophilic chitosan-cellulose sponges was used as carrier for cubosomal nanoparticle. The sponges show great water absorption capacity and quick shape recovery. Accordingly, these findings confirmed the cubosomal sponge as a successful tool for the topical delivery of β-sitosterol with single daily dose instead of repeated dosing regimen. Thus, leading to an increase of patient adherence and the subsequent better management of burn wound. *In vivo* study results showed that β-sito-cubs sponge was successful in the treatment of thermal burn by enhancing β-sitosterol activity through increasing its skin penetration and keep the burn moisture which may result in better patient compliance and excellent healing results in comparison with the commercially available product.

Author Contributions Abeer Khattab: The conception, acquisition, design, analysis, interpretation of data for the work, drafting of the work and final approval of the version to be published. Soha Ismail: The conception, acquisition, design, analysis, interpretation of data for the work, drafting of the work and final approval of the version to be published. Areeg Abdelrazek: The design, analysis, interpretation of data for the work, drafting of the work.

Funding Open access funding provided by The Science, Technology & Innovation Funding Authority (STDF) in cooperation with The Egyptian Knowledge Bank (EKB). This research did not receive any specific grant from funding agencies in the public, commercial, or not-for-profit sectors.

Declarations

Conflict of Interest The authors declare that no potential conflicts of interest.

References

1. Abbas M, Al-Rawi N, Abbas M, Al-Khateeb I. Naringenin potentiated β-sitosterol healing effect on the scratch wound assay. Res Pharm Sci. 2019;14(6):566–73. https://doi.org/10.4103/1735-5362.272565.
2. Sun Y, Gao L, Hou W, Wu J. β-Sitosterol Alleviates Inflammatory Response via Inhibiting the Activation of ERK/p38 and NF-κB Pathways in LPS-Exposed BV2 Cells. Biomed Res Int. 2020;2020:7532306. https://doi.org/10.1155/2020/7532306.
3. Jewo PI, Fadeyibi IO, Babalola OS, Saalu LC, Benebo AS, Izegbu MC, Ashiru OA. A comparative study of the wound healing properties of Moist Exposed Burn Ointment (MEBO) and silver sulphadiazine. Ann Burns Fire Disasters. 2009;22(2):79–82.
4. Bakr MM, Shukr MH, ElMeshad AN. In situ hexosomal gel as a promising tool to ameliorate the transnasal brain delivery of vinpocetine: Central composite optimization and in vivo biodistribution. J Pharm Sci. 2020;109(7):2213–23. https://doi.org/10.1016/j.xphs.2020.03.030.
5. Salentinig S, Sagalowicz L, Glatter O. Self-assembled structures and pK a value of oleic acid in systems of biological levance. Langmuir. 2010;26(14):11670–9. https://doi.org/10.1021/la101012a.
6. Kaur N, Garg T, Goyal AK, Rath G. Formulation, optimization and evaluation of curcumin-β-cyclodextrin-loaded sponge for effective drug delivery in thermal burns chemotherapy. Drug Deliv. 2016;7:2245–54. https://doi.org/10.3109/10717544.2014.963900.
7. Milak S, Zimmer A. Glycerol monooleate liquid crystalline phases used in drug delivery systems. Int J Pharm. 2015;478(2):569–87. https://doi.org/10.1016/j.ijpharm.2014.11.072.
8. RezvaniGhomi E, Khalili S, Nouri Khorasani S, EsmaeelyNeisiany R, Ramakrishna S. Wound dressings: Current advances and future directions. J Appl Polym Sci. 2019;136:47738.
9. Kheirabadi BS, Mace JE, Terrazas IB, Fedyk CG, Estep JS, Dubick MA, Blackbourne LH. Safety evaluation of new hemostatic agents, smectite granules, and kaolin-coated gauze in a vascular injury wound model in swine. J Trauma Acute Care. 2010;68:269–78.
10. Englehart MS, Cho SD, Tieu BH, Morris MS, Underwood SJ, Karahan A, Schreiber MA. A novel highly porous silica and chitosan-based hemostatic dressing is superior to HemCon and gauze sponges. J Trauma Acute Care. 2008;65:884–90.
11. Zietlow JM, Zietlow SP, Morris DS, Berns KS, Jenkins DH. Prehospital use of hemostatic bandages and tourniquets: translation from military experience to implementation in civilian trauma care. J Spec Oper Med. 2015;15:48–53.
12. Fan X, Li M, Yang Q, Wan G, Li Y, Li N, Tang K. Morphology-controllable cellulose/chitosan sponge for deep wound hemostasis with surfactant and pore-foaming agent. Mater Sci Eng C Mater Biol Appl. 2021;118:111408. https://doi.org/10.1016/j.msec.2020.111408.
13. Gaballa S, El Garhy O, Abdelkader H. Cubosomes: composition, preparation, and drug delivery applications. J Adv Biomed Pharm Sci. 2020;3:1–9.
14. Shaker D, Ismail S, Hamed S, El-Shishtawy E. Butoconazole nitrate vaginal sponge: Drug release and antifungal efficacy. J Drug Del Sci Technol. 2018;48:274–87.
15. Fan XL, Chen KK, He XC, Li N, Huang JB, Tang KY, Wang F. Nano-TiO2/ collagen-chitosan porous scaffold for wound repairing. Int J Biol Macromol. 2016;91:15–22.
16. He XC, Fan XL, Feng WP, Chen Y, Guo T, Wang F, Tang KY. Incorporation of microfibrillated cellulose into collagen-hydroxyapatite scaffold for bone tissue engineering. Int J Biol Macromol. 2018;115:385–92.
17. Khattab A, Shalaby S. Optimized ciclopirox-based eudragit RLPO nail lacquer: Effect of endopeptidase enzyme as permeation enhancer on transungual drug delivery and efficiency against onychomycosis. AAPS Pharm Sci Tech. 2018;19:1048–60. https://doi.org/10.1208/s12249-017-0917-8.
18. Morsi N, Abdelbary G, Ahmed M. Silver sulfadiazine based cubosome hydrogels for topical treatment of burns: Development and in vitro/in vivo characterization. Eur J Pharm Biopharm. 2014;86(2):178–89.
19. Alblesh HA. Wound healing efficacy of dexpanthenol versus beta-sitosterol: A comparative study in a rat model. Int J Pharm Bio Med Sci. 2024;4(2):49–58.
20. Karatepe M. Simultaneous determination of ascorbic acid and free malondialdehyde in human serum by HPLC – UV. LCGC Asia Pacyfic. 2004;7(2):7–9.
21. Jayatilleke E, Shaw S. A high-performance liquid chromatographic assay for reduced and oxidized glutathione in biological samples. Anal Biochem. 1993;214(2):452–7. https://doi.org/10.1006/abio.1993.1522.
22. Kunchi Z, Shaowa LV, Xiuyan L, Yufei F, Xin L, Lu L, Shuang L, Yongji L. Preparation, characterization, and in vivo pharmacokinetics of nanostructured lipid carriers loaded with oleanolic acid and gentiopicrin. Int J Nanomed. 2013;8:3227–39. https://doi.org/10.2147/IJN.S45031.
23. Nakano M, Teshigawara T, Sugita A, Leesajakul W, Taniguchi A, Kamo T, Handa T. Dispersions of liquid crystalline phases of the Monoolein/Oleic Acid/Pluronic F127 System. Langmuir. 2002;18(24):9283–8. https://doi.org/10.1021/la026297.
24. Danaei M, Dehghankhold M, Ataei S, HasanzadehDavarani F, Javanmard R, Dokhani A, Khorasani S, Mozafari M. Impact of particle size and polydispersity index on the clinical applications of lipidic nanocarrier systems. Pharmaceutics. 2018;10(2):57. https://doi.org/10.3390/pharmaceutics10020057.
25. BintiRosli NS, Rahman AA, Aziz AA, Shamsuddin S, Ibrahim AR. The effect of gold nanoparticle size in the cellular uptake. Solid State Phenomena. 2019;290:75–80.
26. FDA—Liposome Drug Products; Chemistry, Manufacturing, and Controls; Human Pharmacokinetics and Bioavailability; Labeling Documentation. Guidance for Industry; April 2018 Pharmaceutical Quality/CMC.; U.S. Department of Health and Human Services Food and Drug Administration Center for Drug Evaluation and Research (CDER): Silver Spring, MD, USA, 2018.
27. Kelidari HR, Saeedi M, Akbari J, et al. Development and optimisation of spironolactone nanoparticles for enhanced dissolution rates and stability. AAPS Pharm Sci Tech. 2017;18:1469–74. https://doi.org/10.1208/s12249-016-0621-0.
28. Bodratti AM, Alexandridis P. Formulation of poloxamers for drug delivery. J Funct Biomater. 2018;9:11. https://doi.org/10.3390/jfb9010011.
29. Morgan NH, Arakeep HM, Haiba DA, Aboelgoud MA. Role of Masson's trichrome stain in evaluating the effect of platelet-rich plasma on collagenesis after induction of thermal burn in adult male albino rats. Tanta Med J. 2022;50(2):86. https://doi.org/10.4103/TMJ.TMJ_128_21.

30. Guo SX, Jin YY, Fang Q, You CG, Wang XG. Beneficial effects of hydrogen-rich saline on early burn-wound progression in rats. PLOS ONE. 2015;10(4):e0124897. https://doi.org/10.1371/journal.pone.0124897.
31. Liao PC, Lai MH, Hsu KP, Kuo YH, Chen J, Tsai MC, Li CX, Yin XJ, Jeyashoke N, Chao LKP. Identification of β-Sitosterol as in vitro anti-inflammatory constituent in moringa oleifera. J Agric Food Chem. 2018;66(41):10748–59. https://doi.org/10.1021/acs.jafc.8b04555.
32. Guo HF, Ali RM, Hamid RA, Zaini AA, Khaza'ai H. A new model for studying deep partial-thickness burns in rats. Int J Burns Trauma. 2017;7(6):107–14.
33. Rowan MP, Cancio LC, Elster EA, Burmeister DM, Rose LF, Natesan S, Chan RK, Christy RJ, Chung KK. Burn wound healing and treatment: review and advancements. Critical Care. 2015;19(1):243. https://doi.org/10.1186/S13054-015-0961-2.
34. Said A, Wahid F, Bashir K, Rasheed HM, Khan T, Siraj S. Sauromatum guttatum extract promotes wound healing and tissue regeneration in a burn mouse model via up-regulation of growth factors. Pharmaceutical Biology. 2019;57(1):736–43. https://doi.org/10.1080/13880209.2019.1676266.
35. Hassan RF, Kadhim HM. Comparative effects of phenolic extract as an ointment dosage form in inducing wound healing in mice and β-sitosterol in experimentally induced acute wound healing in mice. J Pharm Negat Results. 2022;13(3):194–203.